Cell Reports
Physical Science

CellPress
OPEN ACCESS

Article

Immunoregulatory cryogel-based contact lenses for bacterial keratitis prevention and treatment

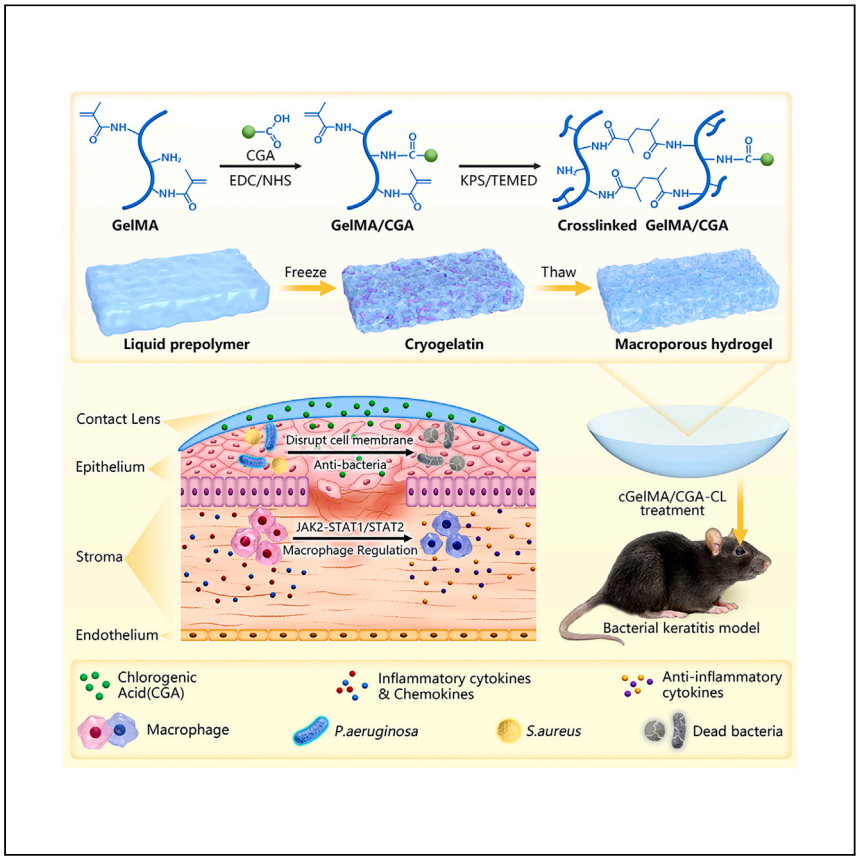

Fan et al. report a macroporous chlorogenic acid (CGA)-conjugated contact lens (CL) based on gelatin methacrylate by cryogelation (cGelMA/CGA-CL) to solve the problems of frequent administration, low bioavailability, and antibiotic resistance in treating bacterial keratitis (BK). Biological experiments confirm that a cGelMA/CGA-CL exhibits excellent biocompatibility with antimicrobial and immunomodulatory properties in BK treatment.

Yuzhuo Fan, Fanfan Chen, Wanzhong Yuan, ..., Mingwei Zhao, Xu Zhang, Kai Wang

zhangxulove@bjmu.edu.cn (X.Z.)
wang_kai@bjmu.edu.cn (K.W.)

Highlights

A macroporous chlorogenic acid (CGA) contact lens (CL) material

Enhanced biocompatibility and antibacterial and immunomodulatory activity

Demonstrated antibiotic resistance in bacterial keratitis treatment

This material may also be extended to the treatment of other infectious diseases

Fan et al., Cell Reports Physical Science 5, 102179
September 18, 2024 © 2024 The Authors. Published by Elsevier Inc.
https://doi.org/10.1016/j.xcrp.2024.102179

Cell Reports
Physical Science

CellPress
OPEN ACCESS

Article

Immunoregulatory cryogel-based contact lenses for bacterial keratitis prevention and treatment

Yuzhuo Fan,[1,2,3,4,10] Fanfan Chen,[5,6,7,8,10] Wanzhong Yuan,[9] Yuchun Sun,[5,6,7] Jiarui Li,[2,3,4] Yan Li,[2,3,4] Mingwei Zhao,[1,2,3,4] Xu Zhang,[5,6,7,*] and Kai Wang[1,2,3,4,11,*]

SUMMARY

Contact lens (CL)-associated bacterial keratitis (BK), a prevalent and underestimated disorder caused by unhygienic CL wear, poses a risk to permanent loss of visual acuity. Clinically, low drug-delivery efficiency, frequent administration, hormone complications, and antibiotic resistance remain the major unsolved challenges. Here, we introduce a chlorogenic acid (CGA)-conjugated CL material based on gelatin methacrylate via cryogelation(cGelMA/CGA-CL) to strengthen the prevention and treatment of BK. The cGelMA/CGA-CL features a highly moist, macroporous, adjustable structure for sustained release of CGA and is favorably biocompatible to cells, providing antimicrobial protection against opportunistic pathogens and inhibiting excessive ocular inflammatory responses through the JAK2-STAT1/STAT2 signaling pathway. Furthermore, the cGelMA/CGA-CL effectively alleviates the symptoms of BK with immunoregulation of macrophage recruitment and anti-inflammatory factor release in a mouse model of BK. The cGelMA/CGA-CL offers a promising candidate for the prevention and treatment of BK, which may significantly reduce the risk of infection for CL wearers.

INTRODUCTION

There are hundreds of millions of contact lens (CL) wearers worldwide.[1,2] At the same time, the use of multifocal soft CLs, but not conventional soft CLs, as a functional myopia control strategy has increased in young adolescents.[3,4] Although generally well tolerated, many unhygienic practices can lead to corneal infections.[5] The risk for bacterial keratitis (BK) is 80 times higher for CL wearers than that for non-CL wearers.[6] The approximate annual incidence of microbial keratitis ranges from two to 20 cases per 10,000 wearers,[7] and CL wear accounts for 52%–65% of new cases, including severe BK, which may result in vision loss, significant costs, and increased morbidity.[8–10] In particular, when there is a defect in the corneal epithelial cell layer and a disturbance in the tear-flushing mechanism, along with the presence of pathogens in sufficient numbers, there is a significant increase in the occurrence of CL-associated BK and the safety risks posed by conventional CL materials. Therefore, CL-associated BK imposes substantial public health and economic burdens,[11,12] and it is imperative to build CL materials with antibacterial or anti-inflammatory properties for BK prevention and treatment.

The most common clinical treatments for BK are antibiotics and hormone-containing anti-inflammatory eye drops.[9] However, these treatments are recommended only when BK is present and cannot be applied as a regular strategy for BK prevention, let alone frequent administration, low bioavailability, increased intraocular pressure

[1]Institute of Medical Technology, Peking University Health Science Center, Beijing, China

[2]Department of Ophthalmology & Clinical Center of Optometry, Peking University People's Hospital, Beijing 100044, China

[3]College of Optometry, Peking University Health Science Center, Beijing, China

[4]Eye Disease and Optometry Institute, Peking University People's Hospital, Beijing, China

[5]Center of Digital Dentistry, Faculty of Prosthodontics, Peking University School and Hospital of Stomatology, Beijing 100081, China

[6]National Engineering Research Center of Oral Biomaterials and Digital Medical Devices, Peking University School and Hospital of Stomatology; Beijing 100081, China

[7]National Center of Stomatology, National Clinical Research Center for Oral Diseases, NHC Key Laboratory of Digital Stomatology, Beijing Key Laboratory of Digital Stomatology, Key Laboratory of Digital Stomatology, Chinese Academy of Medical Sciences, Peking University School and Hospital of Stomatology; Beijing 100081, China

[8]Department of Stomatology, Beijing Shijitan Hospital, Capital Medical University, Beijing, China

[9]Department of Neurosurgery, Beijing Friendship Hospital, Capital Medical University, Beijing, China

[10]These authors contributed equally

[11]Lead contact

*Correspondence:
zhangxulove@bjmu.edu.cn (X.Z.),
wang_kai@bjmu.edu.cn (K.W.)

https://doi.org/10.1016/j.xcrp.2024.102179

This is an open access article under the CC BY-NC-ND license (http://creativecommons.org/licenses/by-nc-nd/4.0/).

due to hormone use, and antibiotic resistance.[13,14] Moreover, traditional eye drops exhibit limited efficiency for severe corneal infections.[15] Despite recent proposals for therapeutic bioproducts or treatment strategies for BK infections, such as metal or metal oxide nanoparticles (Au, Ag, and TiO_2) incorporated into hybrid hydrogels,[16] DNA nanogels loaded with bioactive peptides (L12 peptide),[17] the near-infrared light-responsive nanoplatforms integrated with nitric oxide (NO),[18] they have inadequately addressed these multifaceted challenges due to their interference in the electrical activity of the optic nerve network,[19,20] mono-functional effect (antibacterial only), and complicated administration with high cost, respectively. Therefore, it is urgent to develop a safe and multifunctional CL material capable of preventing infections during daily wear and providing effective treatment in the event of ocular infection.

Chlorogenic acid (CGA), a polyphenolic compound found in honeysuckle, eucommia, chrysanthemum, and coffee, exhibits various pharmacological activities, including antibacterial, antioxidant, anti-inflammatory, and free-radical-scavenging effects.[21] A recent study indicated that CGA induced cell death in pathogenic bacterial strains, including *Shigella dysenteria* and *Streptococcus pneumoniae*, by prompting irreversible permeability changes in the cell membrane, causing cells to lose their ability to maintain membrane potential and cytoplasm macromolecules, including nucleotides.[22] Moreover, CGA can improve microbiota composition and alleviate inflammatory diseases, which manifest enhanced antioxidant enzymes and suppressed inflammatory cytokines.[23–25] However, the significant interindividual variations in the utilization and metabolism of CGA in basic and clinical studies present notable limitations, hindering its clinical application without modifications.[26,27] Li et al. loaded CGA onto poly(D,L-lactide-co-glycolide) (PLGA) and modified them with polyvinylpyrrolidone (PVP) for sustained CGA release to alleviate bone loss in mouse periodontitis.[28] Alternately, macroporous cryogel is fabricated by a hydrogel precursor solution at subzero temperatures (cryogelation), which provides a highly moist environment comprising a high water content and facilitates the rapid exchange of oxygen and metabolic wastes owing to their inherent interconnected macroporous network.[29–32] Additionally, the dense polymer walls of cryogels can efficiently entrap biomolecules.[33,34] These features make cryogels a highly attractive scaffold material for CL. However, designing and manufacturing a cryogel system with controlled binding and release properties of biomolecules remains challenging.[35] In particular, the burst release of biomolecules is consistently reported as a major limitation for developing cryogel-based delivery systems.[30]

To address the challenges outlined above, here we develop a multifunctional CL (CL based on gelatin methacrylate via cryogelation [cGelMA]/CGA) material to prevent and address the issues of CL-associated BK (Scheme 1). This therapeutic CL material consists of a macroporous cryogel-based GelMA scaffold conjugated with a biocompatible concentration of CGA for a sustainable and controlled-release delivery system. The results of both *in vitro* and *in vivo* experiments suggest that the cGelMA/CGA-CLs exhibit excellent biocompatibility with antimicrobial and anti-inflammatory properties. Under infectious conditions, the cGelMA/CGA-CLs reveal effective therapeutic and recovery effects on the corneal tissue through the JAK2-STAT1/STAT2 signaling pathway for regulating macrophage recruitment and inflammatory factor release. In summary, cGelMA/CGA-CLs provide a promising CL scaffold material with an integrated prevention and treatment function, and significantly reduce the CL-associated infectious risks to alleviate the associated public health burdens.

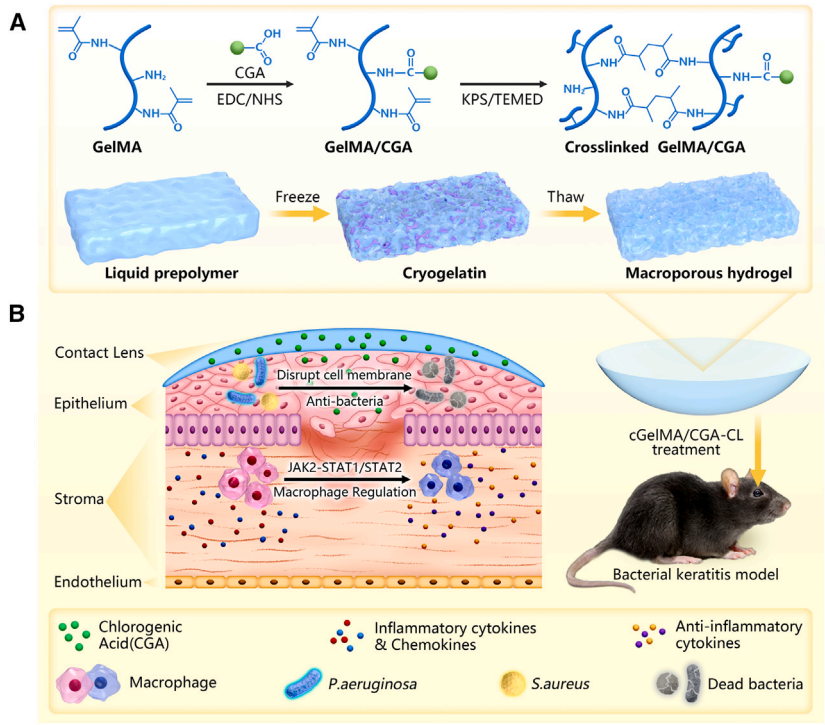

Scheme 1. Immunoregulatory cryogel-based CL for preventing and treating CL-associated bacterial keratitis

(A) Schematic of cGelMA/CGA synthesis. Chlorogenic acid (CGA) was grafted onto gelatin methacrylate (GelMA) via the conjugating agent NHS/EDC, followed by cryogelation, resulting in crosslink formation between methacrylate groups in the presence of radical initiators. Ice crystals formed during the freezing and thawing process after cryogelation resulting in the formation of a hydrogel with macro-scale pores.

(B) Immunoregulation and antibacterial procession of the cGelMA/CGA-CL in bacterial keratitis (BK) wounds. Antibacterial effect of cGelMA/CGA-CL in corneal tissues of C57BL/6J mice with BK by disrupting bacterial cell membranes and anti-inflammatory effect by inhibiting the JAK2-STAT1/STAT2 signaling pathway.

RESULTS

Preparation and characterization of the cGelMA/CGA

The macroporous CGA-conjugated cryogel based on methacrylated gelatin (cGelMA/CGA) was fabricated according to the process shown in Scheme 1A cGelMA/CGA_{100}, cGelMA/CGA_{200}, and cGelMA/CGA_{300} had CGA contents of 100, 200, and 300 mM, respectively, whereas the 10% blank gelatin methacrylate via cryogelation (cGelMA) served as the control group. The homogeneous solution and crosslinked hydrogel after cryogelation were characterized using the vial tilting method (Figure 1A). The scanning electron microscope (SEM) images indicated that all cryogels had interconnected porous structures, and the pore sizes of cGelMA/CGA_{200} and cGelMA/CGA_{300} were larger than those of cGelMA and cGelMA/CGA_{100} (Figure 1B). As the concentration of CGA increased, it occupied more amino groups and reduced the network structure's crosslinking density. Fourier transform infrared (FTIR) spectrum was carried out to determine the grafting mode (Figure 1C). Compared with that of GelMA, the peak value of N–H stretching of GelMA/CGA shifted from 3,396 to 3,355 cm^{-1}, resulting from an increase in benzene ring–OH stretching of CGA. Furthermore, GelMA/CGA showed a strong increase in the intensity of C=O stretching (1,651 cm^{-1}) and N–H bending (1,545 cm^{-1}), indicating amide

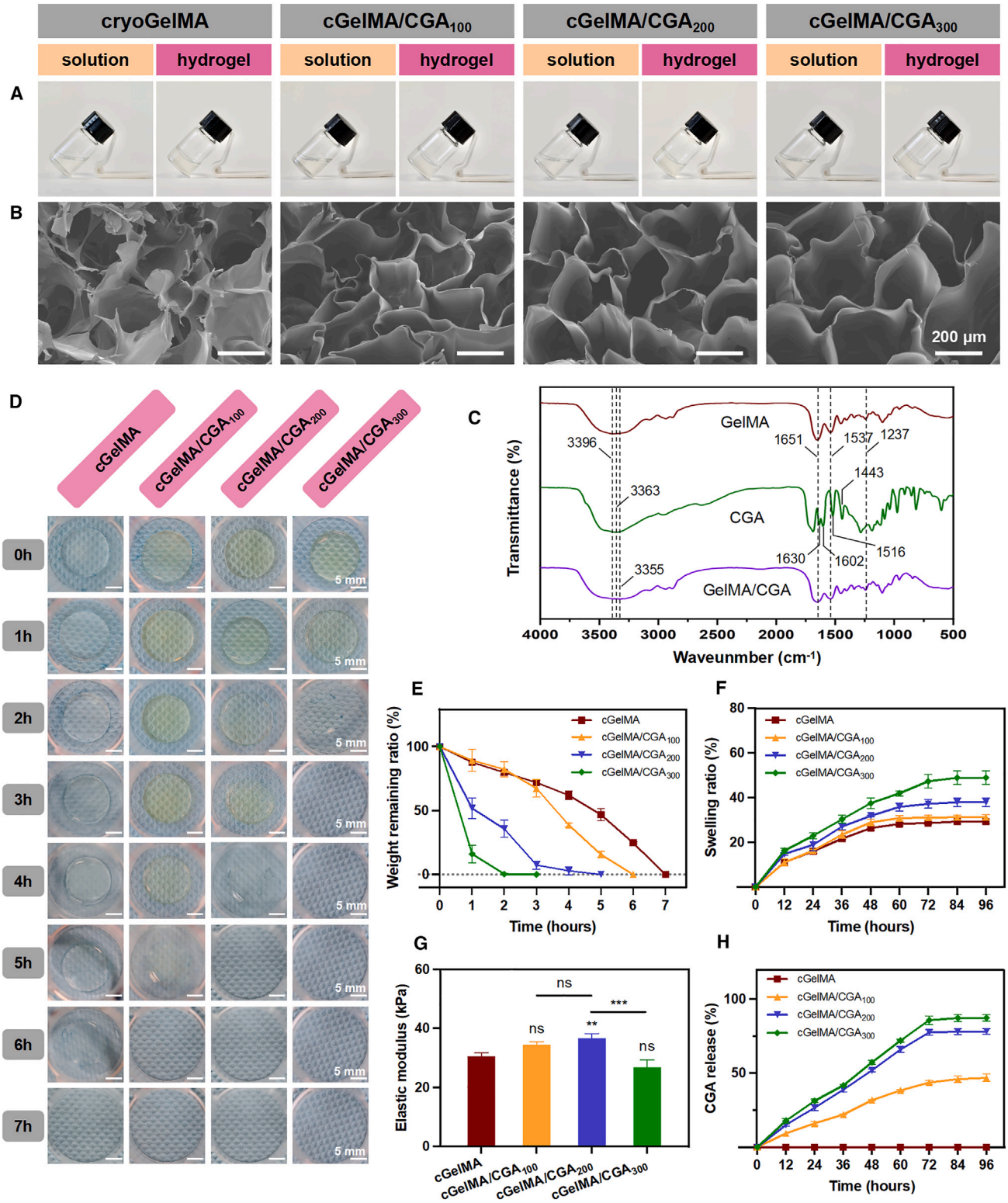

Figure 1. Morphology and characterization of cryogels

(A) cGelMA, cGelMA/CGA_{100}, cGelMA/CGA_{200}, and cGelMA/CGA_{300} solutions before and after cryogelation.

(B) Typical scanning electron microscope (SEM) images of hydrogel cross-sections (scale bar: 200 μm).

(C) Grafting mode results of cryogels via Fourier transform infrared (FTIR) spectra detection.

Figure 1. *Continued*

(D) Representative photos of morphological changes during enzymatic degradation *in vitro* (scale bar: 5 mm).

(E) Weight remaining ratio during enzymatic degradation. Data are represented as mean ± SD.

(F) The swelling curve of cryogels soaked in phosphate-buffered saline (PBS) at pH 7.4 and 37°C. Data are represented as mean ± SD.

(G) Cumulative release of CGA from cGelMA/CGA_{100}, cGelMA/CGA_{200}, and cGelMA/CGA_{300} in PBS at pH 7.4. Data are represented as mean ± SD.

(H) Quantitative analysis of the elastic modulus of cryogels. CGA, CGA. Data are represented as mean ± SD.

bond formation. These results confirmed that CGA was grafted onto GelMA through amide bond formation by conjugation agents.

The equilibrium water content (EWC) of the cryogels was then determined during their incubation in phosphate-buffered saline (PBS) solutions, which ranged between 91.4% and 93.2% (Figure S1) and was comparable to the 85.5% ± 1.5% water content of native human corneas.[36]

The oxygen permeability of the CL is critical for wearers requiring long-term wear to avoid oxygen deprivation of the cornea. In the CL industry, the oxygen permeability is characterized as "Dk," where D is the diffusivity of the lens and k is the oxygen solubility in the lens material. The relationship between the EWC and Dk is[37]

$$Dk = 1.67\, e^{0.0397EWC} \quad \text{(Equation 1)}$$

In Figure S1, the cGelMA/CGA_{200} showed the highest Dk values. Next, the process of wound healing in BK was simulated by immersing cryogels in matrix metalloproteinase-2 (MMP-2) solution.[38] With the addition of CGA, the enzymatic degradation of cGelMA/CGA was accelerated for more amide bonds and decreased crosslinking density of GelMA (Figures 1D and 1E). The degradation rate of four cryogels was as follows: cGelMA/CGA_{300} > cGelMA/CGA_{200} > cGelMA/CGA_{100} > cGelMA, which meant that cGelMA/CGA_{200} could remain on the eyeball for a short period (5 h) for patient safety and comfort in an infectious ocular environment[39] (Figure 1E).

In addition, the elastic modulus of cGelMA/CGA_{200} was 34.60 ± 1.61 kPa, which possessed superior mechanical property to cGelMA (Figure 1G). We postulate that this improvement is the result of noncovalent interactions between the functional groups of gelatin chains and the catechol groups of the CGA as dynamic crosslinking points, such as hydrogen, π, hydrophobic, metal coordination, and electrostatic. Remarkably, the elastic modulus of cryogels did not change when the concentration of CGA was increased from 100 to 200 mM, and it did not begin to decrease until a high concentration of CGA (300 mM) was administered. To characterize the release behavior of CGA from cryogels, we soaked cGelMA, cGelMA/CGA_{100}, cGelMA/CGA_{200}, and cGelMA/CGA_{300} in PBS at pH 7.4 for determining the release volume of CGA within a defined duration. The ε-amino group on cGelMA in our study was 0.13 ± 0.01 mmol/g GelMA, indicating that the theoretical maximum percentage of CGA in cGelMA/CGA conjugate was 13 mM. However, CGA was required in excess to achieve a better grafting effect. The release of CGA from cGelMA/CGA occurred more slowly through dissociation from the main chains and related diffusion processes of free unconjugated CGA, resulting in a slow and sustained release phase (Figure 1H). Notably, the maximum amount of CGA diffused into PBS from different ratios of cGelMA/CGA after 72 h was 45%, 78%, and 82%, respectively. This could be because the conjugation of CGA with GelMA reduced the crosslinking degree of GelMA to increase the average porosity of cGelMA/CGA and facilitate CGA release.

Biosafety evaluation of the cGelMA/CGA

Biocompatibility is an essential property of CLs used in clinical applications.[40,41] We established a cell-cryogel co-culture system in a Transwell chamber using human corneal epithelial cells (HCECs) to investigate the safety of the cryogels *in vitro* (Figure 2A).[42] The Cell Counting Kit-8 (CCK-8) assay demonstrated that the cell viabilities of the cGelMA, cGelMA/CGA_{100}, and cGelMA/CGA_{200} groups were elevated at a predetermined time, compared to that of the blank group without any material, indicating that the formulated cryogels promoted cell proliferation (Figure 2B). However, the cell viability decreased in the cGelMA/CGA_{300} group compared to that in the control group, demonstrating that this concentration was toxic to the cells (Figure 2B). Furthermore, a live/dead staining assay was performed after 1 and 7 days to assess the short-term and long-term toxicity of cryogels to cells. The proportions of green fluorescence (live cells) in the blank, cGelMA, cGelMA/CGA_{100}, and cGelMA/CGA_{200} groups were similar on day 1 and day 7 (Figures 2C and S2), suggesting that the cryogels (except for cGelMA/CGA_{300}) provided sustained support for both cell adhesion and growth. The morphology of HCECs was observed after 1 and 3 days of co-incubation with different cryogels using fluorescence staining. When HCECs were co-cultured with cryogels for 1 and 3 days, the cytoskeleton of HCECs exhibited a more regular pentagonal or hexagonal shape with a tight and regular arrangement in the blank, cGelMA, cGelMA/CGA_{100}, and cGelMA/CGA_{200} groups (Figure 2D). However, some local cytoskeletons began to deform, became more acute, showed protruded pseudopods, and were less regularly arranged after 1 and 3 days in the cGelMA/CGA_{300} group. Altogether, these findings suggested that cGelMA, cGelMA/CGA_{100}, and cGelMA/CGA_{200} exhibited favorable biosafety and supported cell adhesion, growth, and proliferation *in vitro*.

To verify the biocompatibility of the cryogels *in vivo*, cGelMA/CGA_{200} was implanted into the dorsal skin of healthy mice. The hematoxylin and eosin (H&E) staining results suggested that no obvious tissue damage or pathological changes, such as inflammation, necrosis, or metaplasia, were induced by cGelMA/CGA_{200} in the major organs (mouse heart, liver, spleen, lung, and kidney tissues) compared to those in normal tissue after 7 days (Figure 2E). These results demonstrated that cGelMA/CGA_{200} shows favorable biosafety *in vitro* and *in vivo*.

Antibacterial activity of the cGelMA/CGA

Staphylococcus aureus (gram-positive) and *Pseudomonas aeruginosa* (gram-negative) are two common and representative pathogens of BK.[8] The number of re-cultivated colony-forming units (CFU) on agar plates showed that there was no significance between blank control and cGelMA group. However, co-culture of the CGA-conjugated cryogels with these bacterial suspensions for 24 h clearly confirmed the antibacterial activity (Figures 3A and 3B), and the quantitative analysis showed that cGelMA/CGA_{200} exhibited significantly different activities against both bacteria ($p < 0.0001$) (Figures 3C and 3D).

The *in vitro* antibacterial effects described above were further verified using a live/dead bacterial staining assay to characterize the membrane permeability of planktonic microbes. Compared to the bacteria with intense green fluorescence in the blank group, most bacteria in the cGelMA/$CGA_{200\&300}$ treatment groups were labeled red or yellow, and only a few green spots appeared, demonstrating a stronger antibacterial efficacy than that of cGelMA/CGA_{100} (Figures 3E and 3F).

The long-term antibacterial properties of cGelMA/CGA were determined after incubation for up to 48 h. The antibacterial effects of cGelMA/CGA on *S. aureus* and

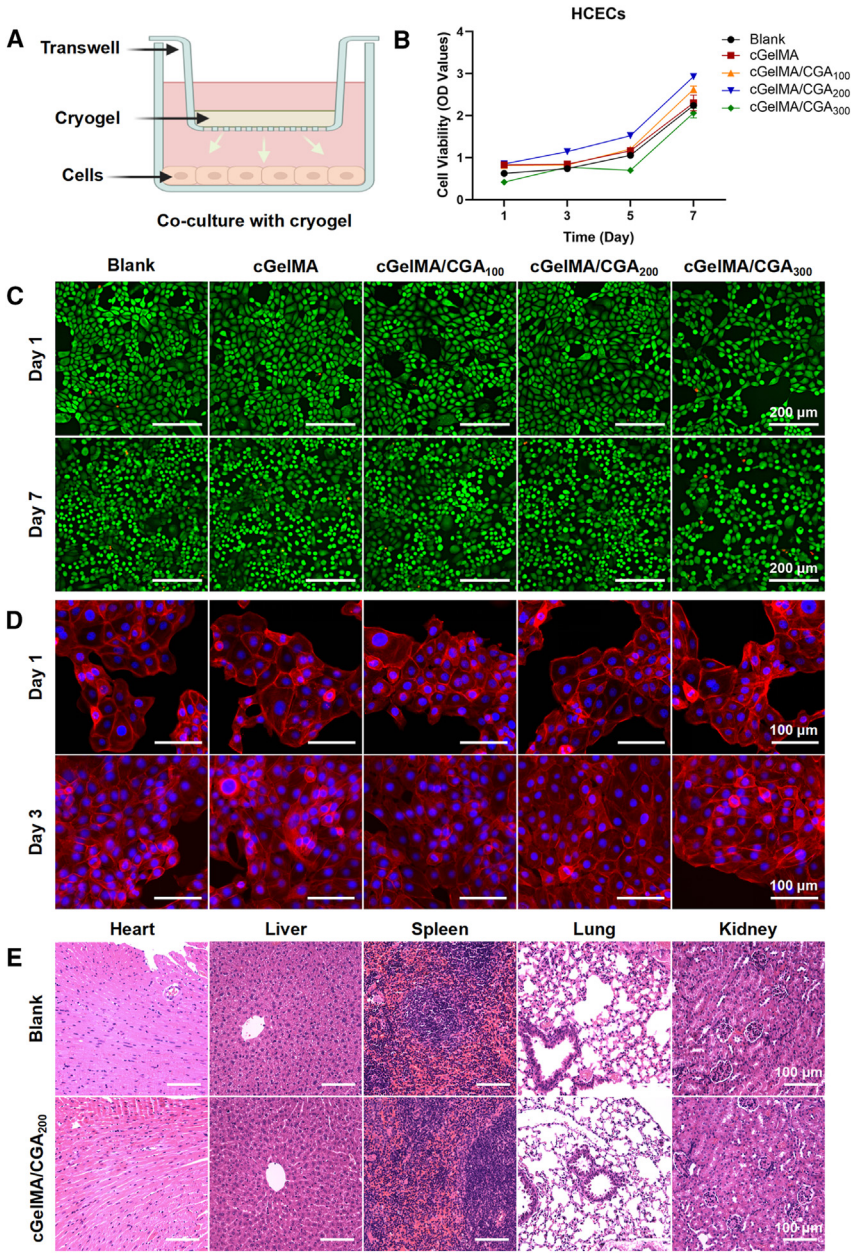

Figure 2. Biosafety evaluation of cryogels

(A) Illustration of the cell-cryogel co-culture model.

(B) Cell Counting Kit-8 (CCK-8) assay of human corneal epithelial cells (HCECs) co-cultured with different cryogels after 1, 3, 5, and 7 days.

(C) Live/dead cell staining of HCECs by incubating with different cryogels for 1 and 7 days (scale bar: 200 μm).

(D) Morphology of HCECs with the incubation of different cryogels after 1 and 3 days. The blue and red colors indicate the cell nucleus and cytoskeleton, respectively (scale bar: 100 μm).

(E) Hematoxylin and eosin (H&E) staining of the heart, liver, spleen, lungs, and kidney in the blank control and cGelMA/CGA_{200} groups (scale bar: 100 μm).

P. aeruginosa became significant and remained steady after 24 h (Figures 3G and 3H). This indicated that cGelMA/CGA continuously maintained its antibacterial activity until degradation. The antibacterial activity of cGelMA/CGA_{100} against

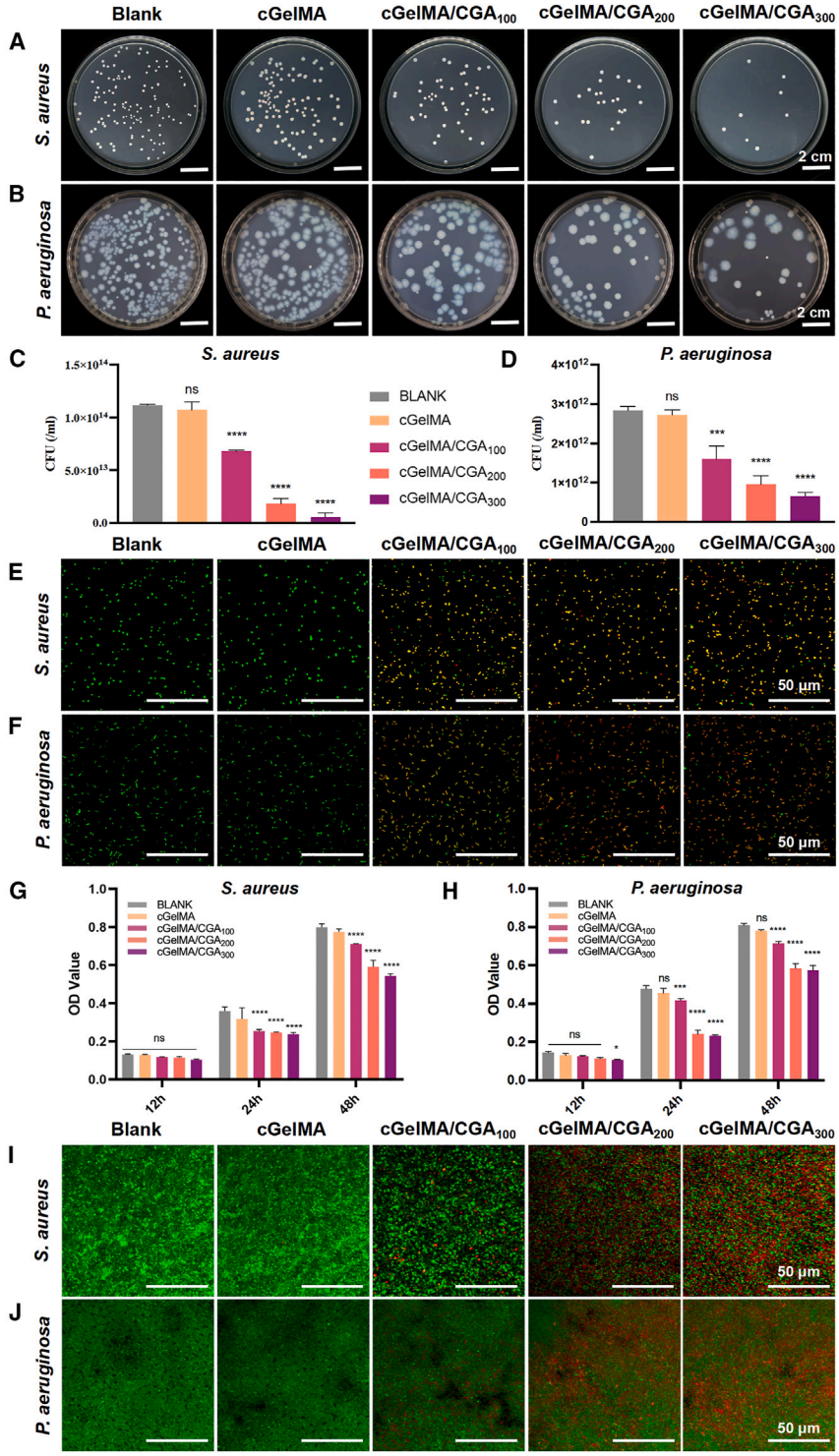

Figure 3. Antibacterial effects of cGelMA/CGA$_{200}$ against *S. aureus* and *P. aeruginosa in vitro*

(A and B) Typical photographs of *S. aureus* and *P. aeruginosa* agar plates after incubation with different cryogels for 24 h (scale bar: 2 cm).

(C and D) Corresponding quantitative histogram of colony-forming unit (CFU) amount. Data are represented as mean ± SD.

Figure 3. *Continued*
(E and F) Live/dead staining images of *S. aureus* and *P. aeruginosa* after different treatments. Living/dead cells are stained with green/red fluorescence, respectively (scale bar: 50 μm).
(G and H) Longevity and stability of antibacterial activity of CGA-loaded cryogels after incubation for 12, 24, and 48 h. Data are represented as mean ± SD.
(I and J) Live/dead staining images of *S. aureus* and *P. aeruginosa* biofilms with various treatments. $^{*}p < 0.05$, $^{**}p < 0.01$, $^{***}p < 0.001$, and $^{****}p < 0.0001$ (scale bar: 50 μm).

P. aeruginosa was lower than that of other cryogels with higher CGA concentrations. The conjugated CGA endowed the cryogel with outstanding antibacterial properties, making it promising for the treatment of BK. In summary, cGelMA/CGA_{200} showed the best overall performance, with excellent biocompatibility and significant antibacterial properties ($p < 0.0001$).

We further tested its feasibility for biofilm eradication using live/dead staining kits. Biofilms are more difficult to eliminate than planktonic bacteria because of the extracellular polymeric substances to shield from antimicrobial agents. In the control group, the mature biofilms of *S. aureus* and *P. aeruginosa* showed a dense green color, which were connected by a large number of live bacteria into a sheet structure, while the dead red bacteria were difficult to observe in the sheet mature biofilm. However, in the experimental group, the biofilms of *S. aureus* and *P. aeruginosa* appeared obviously destroyed, and the live bacteria no longer gathered into sheets and scattered in the visual field. At the same time, a larger number of red dead bacteria appeared (Figures 3I and 3J).

Macrophage-targeted immune regulation property of cGelMA/CGA *in vitro*

Mature human leukemia monocytic (THP-1) cells were induced into an inflammatory state with lipopolysaccharide (LPS), to mimic *in vivo* macrophage activation in BK wounds, followed by treatment with different cryogels. All cryogel-treated groups showed reduced expression of BK inflammation-related genes (cytokines interleukin [IL]-6, IL-12, chemokine CCL4, CCL5, and CXCL10) and significantly increased expression of anti-inflammatory gene (IL-10) compared to the LPS group, as demonstrated via reverse transcription quantitative PCR (RT-qPCR) results (Figure 4A). These results suggested that different concentrations of CGA inhibited the expression of inflammatory cytokines and chemokines in LPS-induced THP-1 cells and increased the expression of anti-inflammatory factors. However, the anti-inflammatory effect did not show a tendency to increase with increasing CGA concentration in the cryogel-treated groups. The cGelMA/CGA_{200} group showed the best anti-inflammatory effects ($^{****}p < 0.0001$; Figure 4A). The cGelMA/CGA_{300} group with higher concentration of CGA showed poorer anti-inflammatory performance compared to the cGelMA/CGA_{200} group (Figure 4A). These results, combined with those of biocompatibility assays, indicated that the cytotoxicity of cGelMA/CGA_{300} led to a decrease in cell activity, thereby affecting anti-inflammatory effects.[43]

Further, the molecular mechanism underlying the action of cGelMA/CGA_{200} cryogel in BK was investigated using RNA sequencing (RNA-seq) to assess the changes in messenger RNA (mRNA) levels in macrophages under the inflammatory conditions for 24 h. A total of 1,530 genes were downregulated and 1,303 were upregulated in the cGelMA/CGA_{200} group compared to those in the LPS control group (Figure 4B).

Gene Ontology (GO) and Kyoto Encyclopedia of Genes and Genomes (KEGG) analysis showed that the cGelMA/CGA_{200} treatment significantly affected the pathways

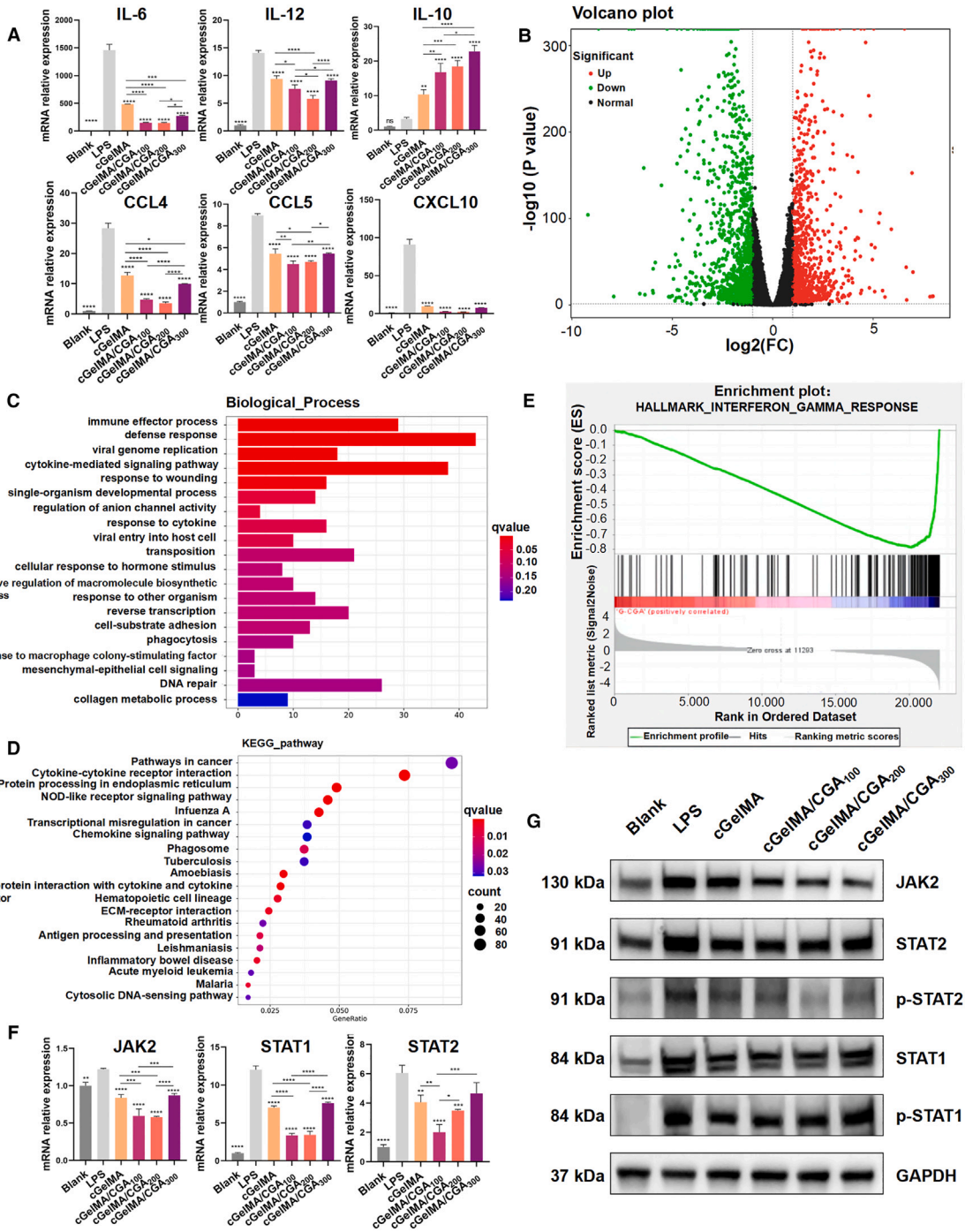

Figure 4. Macrophage-targeted immune regulation property of cGelMA/CGA *in vitro*

(A) Real-time qPCR of bacterial keratitis inflammatory factors in different cryogel treatment groups (n = 3). Data are represented as mean ± SD.

(B) Volcano plot of differentially expressed genes (results were deemed significant if $|\log_2(FC)| \geq 2$ and FDR-corrected $p < 0.05$; three biologically independent replicates were performed for each control or treatment). Black region, not significant; red region, significantly upregulated genes; green region, significantly downregulated genes.

(C) Gene Ontology (GO) analysis of the top 20 terms in biological process (BP) for the cGelMA/CGA_{200} group.

(D) Kyoto Encyclopedia of Genes and Genomes (KEGG) pathway analysis of the top 20 relevant pathways in response to cGelMA/CGA_{200}.

(E) Gene set enrichment analysis (GSEA) of the gene signaling pathways with crucial biological significance.

(F and G) (F) Real-time qPCR (n = 3) and (G) western blot verification of selected genes in different cryogel treatment groups (n = 3~4). Data represent mean ± SD; *$p < 0.05$, **$p < 0.01$, ***$p < 0.001$, and ****$p < 0.0001$.

associated with macrophage immune regulation, including the immune effector process, defense response, and the NOD-like receptor signaling pathway (Figures 4C and 4D). Furthermore, we performed gene set enrichment analysis (GSEA) based on the hallmark gene set from the Human Molecular Signatures Database to localize the gene signaling pathways more precisely with crucial biological significance and meaningful phenotypic differences after cGelMA/CGA_{200} treatment. In the cGelMA/CGA_{200} group, the interferon (IFN)-γ response signaling pathway, related to numerous inflammatory and immune diseases, was significantly negatively regulated (normalized enrichment score [NES] = −3.16, false discovery rate [FDR] $q < 0.0001$, $p < 0.0001$) (Figure 4E). Compelling genetic and biochemical data support key nonredundant roles of Janus kinase 1 (JAK1), Janus kinase 2 (JAK2), signal transducer and activator of transcription (STAT 1/2), and many IFN-stimulated genes in mediating IFN-γ responses and functions, such as modulation of immunity, host defense against intracellular pathogens, and inflammatory responses and associated tissue damage.[44] Meanwhile, JAK-STAT is one of the critical pathways in the pathogenesis of infectious keratitis.[45,46] In this study, *JAK2*, *STAT1*, and *STAT2* were differentially expressed and significantly downregulated in the cGelMA/CGA_{200} group. Therefore, we hypothesized that cGelMA/CGA_{200} could target the JAK2-STAT1/STAT2 signaling pathway in macrophages to alleviate inflammation.

To verify our hypothesis, the expression levels of JAK2, STAT1, and STAT2 were detected using RT-qPCR and western blotting (WB). The mRNA levels of JAK2, STAT1, and STAT2 were significantly decreased in the cryogel-treated groups (Figure 4F). Additionally, the protein expression of JAK2, phosphorylated STAT1/STAT1, and phosphorylated STAT2/STAT2 was significantly decreased in the cryogel-treated groups (Figures 4G; S3). Among these results, the cGelMA/CGA_{200} group showed the greatest downregulation of JAK2-STAT1/STAT2 compared to all other groups. This was consistent with the RT-qPCR results for the inflammatory cytokines and chemokines. Taken together, cGelMA/CGA_{200} could inhibit excessive immune responses by suppressing the expression of the JAK2-STAT1/STAT2 signaling pathway during bacterial infection.

BK treatment *in vivo*

To further explore the BK treatment performance of cGelMA/CGA *in vivo*, a BK animal model was constructed via injecting 5 μL of bacterial suspension (1.0×10^8 CFU/mL, *S. aureus*) into the mechanically injured corneas (right eye) of C57BL/6J mice every 24 h, three times in total (Figure 5A). After successful modeling of BK, appropriately sized (diameter 3–4 mm) CLs were prepared and placed on the eyes of mice and the progression of BK was observed under a slit lamp (Figure 5B). cGelMA/CGA-CL and levofloxacin (LVFX) eye-drop groups had similar clinical scores, which were lower than cGelMA and control groups at 1, 3, 5, and 7 days (Figure 5C). As shown, all groups initially had large corneal ulcers on day 1 (Figures 5D and 5E). There was significant corneal opacity in the central part of the cornea after 7 days, with a rapid increase in signs of infection such as corneal ulcer and interstitial edema, displaying that the ulcerative lesions gradually worsened over time in the untreated control group (Figure 5D). Some corneal opacity and inflammatory infiltration persisted on day 7 in the cGelMA-CL group and damage to the corneal epithelium and superficial stroma remained (Figures 5D and 5E). Significantly, the corneal clarity and transparency of the cGelMA/CGA-CL and LVFX groups rapidly increased, the symptoms of infection disappeared, the damaged corneal epithelium was repaired, and the total clinical score dropped below 1 (Figures 5C–5E). The results revealed that cGelMA/CGA-CL could effectively alleviated the symptoms of BK like the clinical LVFX.

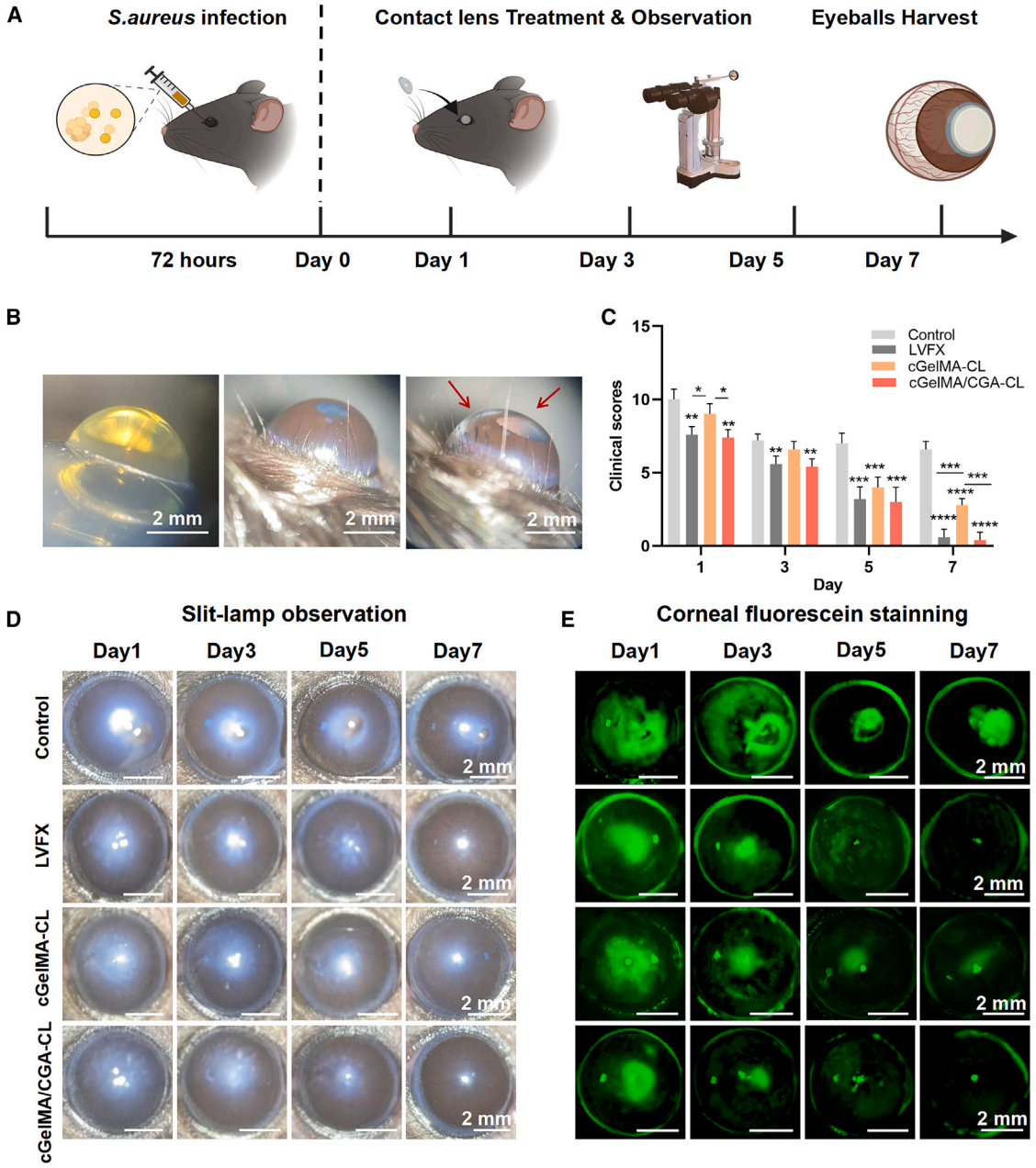

Figure 5. *In vivo* treatment effect of the cGelMA/CGA-CL for BK

(A) Schematic illustration of the construction of BK animal model and treatment procedure.

(B) From left to right, a sample of a cGelMA/CGA-CL made with a 4-mm-diameter mold, a lateral view of the eye of mice without a CL, and a lateral view of the eye of mice with a cGelMA/CGA-CL (the red arrow points to the clear cGelMA/CGA-CL). Scale bar: 2 mm.

(C) Clinical grading scores of different treatments ($n = 5$).

(D) Slit-lamp images of bacteria-infected keratitis model under different treatments on day 1, 3, 5, and 7; Scale bar: 2 mm.

(E) Slit-lamp images of corneal fluorescein stained on day 1, 3, 5, and 7 of the BK models to show the impaired cornea area. (Reduce red and blue channels by 200% in original image to simulate corneal lesion observation with a slit lamp equipped with a yellow filter clinically). Scale bar: 2 mm. Data represent mean ± SD; *$p < 0.05$, **$p < 0.01$, ***$p < 0.001$, and ****$p < 0.0001$.

BK inflammation inhibition

Additionally, the histological analysis of the corneal sections was performed after 7 days of treatment (Figure 6). Severe inflammatory cell infiltration was observed in the H&E-stained images of the control group, the corneal thickness was

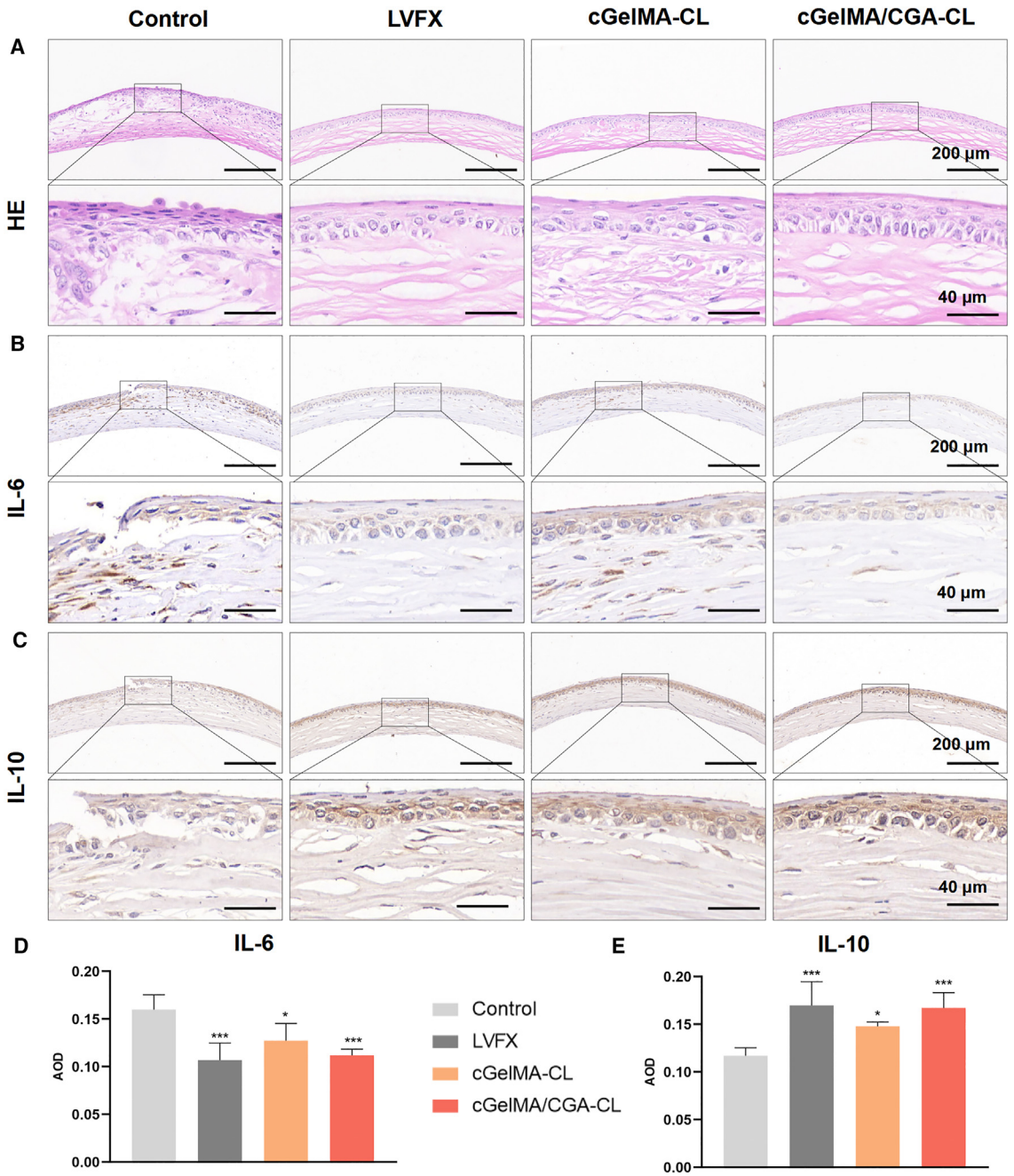

Figure 6. *In vivo* anti-inflammatory properties of cGelMA/CGA-CL ($n = 5$)

(A) H&E staining of the cornea with different treatments on day 7.

(B and C) Immunohistochemical (IHC) staining of IL-6 and IL-10 in each group on day 7, respectively. Scale bar: 200 μm. Scale bar in the enlarged images: 40 μm.

(D and E) Average optical density (AOD) values after positive IHC staining of IL-6 and IL-10. Data are represented as mean ± SD. *$p < 0.05$, **$p < 0.01$, ***$p < 0.001$, and ****$p < 0.0001$.

significantly increased, and the corneal stroma was severely damaged and irregularly aligned (Figure 6A). Moreover, the inflammatory infiltration was relatively reduced in the cGelMA-CL group and the corneal thickness was almost normal compared to the control group. However, the corneal stroma was still damaged and irregularly aligned (Figure 6A). Alternatively, in the cGelMA/CGA-CL and

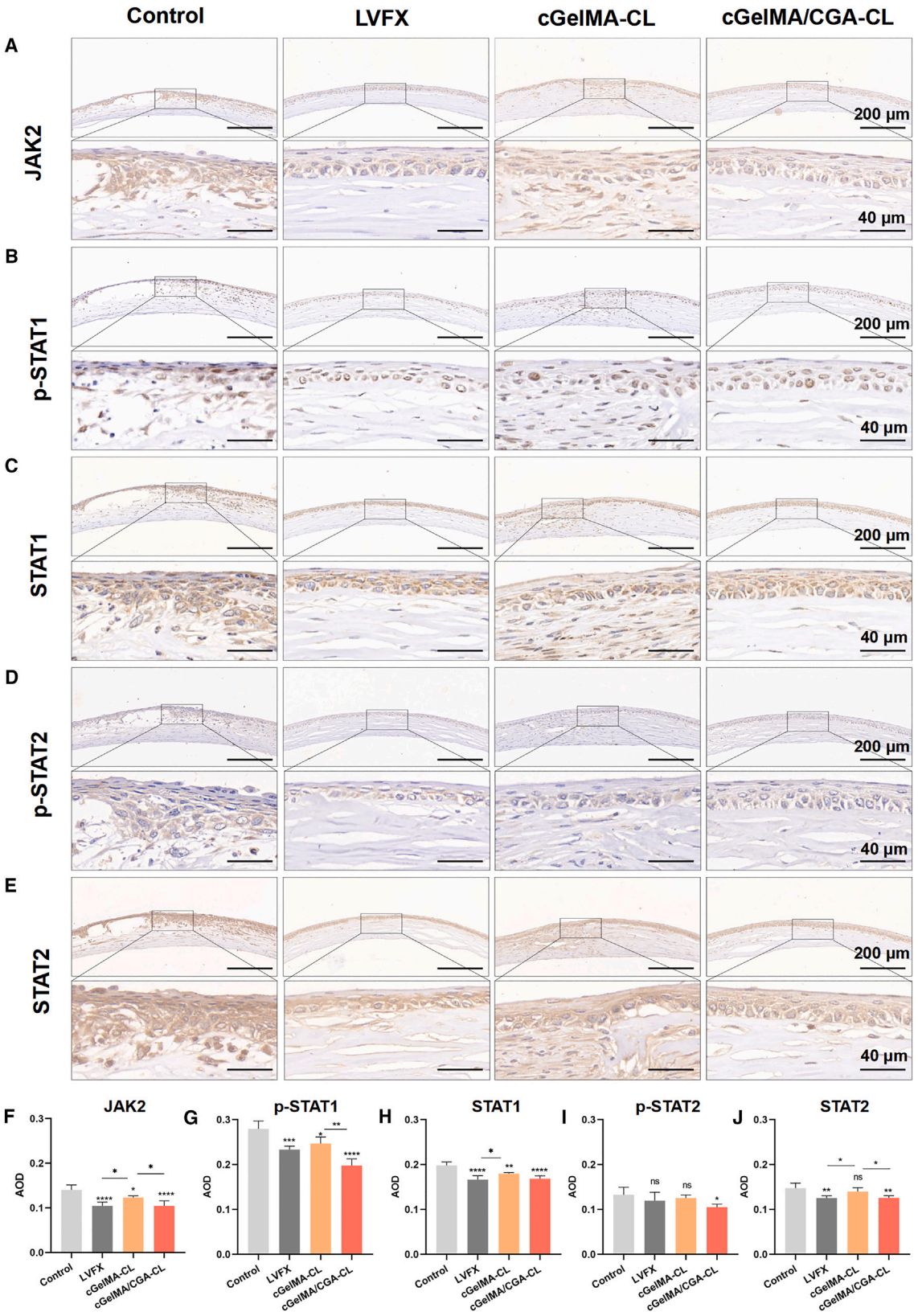
Control
LVFX
cGelMA-CL
cGelMA/CGA-CL
A
JAK2
B
p-STAT1
C
STAT1
D
p-STAT2
E
STAT2
200 μm
40 μm
F
JAK2
G
p-STAT1
H
STAT1
I
p-STAT2
J
STAT2
AOD
0.0
0.1
0.2
0.3
Control
LVFX
cGelMA-CL
cGelMA/CGA-CL
ns

Figure 7. Representative results of the anti-inflammatory signaling pathway of cGelMA/CGA-CL *in vivo* ($n = 5$)

(A–E) IHC staining of JAK2, p-STAT1, STAT1, p-STAT2, and STAT2 in each group on day 7, respectively. Scale bar: 200 μm. Scale bar in the enlarged images: 40 μm.

(F–J) AOD values after positive IHC staining, respectively. Data are represented as mean ± SD. *$p < 0.05$, **$p < 0.01$, ***$p < 0.001$, and ****$p < 0.0001$.

LVFX groups, the results indicated that there was no apparent tissue damage and no visible inflammatory cell infiltration, the corneal epithelium and stroma were intact, and the cells were regularly arranged (Figure 6A).

The inflammatory cytokine IL-6 was highly expressed in the control and cGelMA-CL groups, whereas the anti-inflammatory cytokine IL-10 showed low expression (Figures 6B and 6C). In contrast, the expression of IL-6 was significantly decreased in the cGelMA/CGA-CL and LVFX groups (***$p < 0.001$, Figure 6D), while IL-10 was significantly increased after 7 days of treatment (***$p < 0.001$, Figure 6E) compared to that in the control group. These results indicated that cGelMA/CGA-CL had significant anti-inflammatory properties *in vivo*.

Furthermore, the immunohistochemical staining results showed the downregulation of JAK2, STAT1, and p-STAT1 but not STAT2 and p-STAT2 in the cGelMA-CL group compared to the control group (Figures 7A–7E). Meanwhile, JAK2, STAT1, p-STAT1, STAT2, and p-STAT2 were significantly downregulated upon cGelMA/CGA-CL treatment compared to the control and cGelMA-CL groups (Figures 7F–7J). Altogether, these results suggested that cGelMA/CGA-CLs played a practical role in alleviating BK via inhibition of the JAK2-STAT1/STAT2 signaling pathway to further reduce excessive macrophage recruitment and inflammatory factor release.

DISCUSSION

In this study, we utilized the generally recognized as safe (GRAS) material GelMA and natural CGA to fabricate the immunoregulatory cryogel-based CLs for BK prevention and treatment (Scheme 1). Jiang et al. reported that higher concentrations of CGA-made radicals (acting as prooxidants) may lead to cytotoxicity,[43] which is consistent with our *in vitro* and *in vivo* results that conjugation of CGA on GelMA up to a concentration of 300 μM led to significant cytotoxicity (Figures 2 and 4). Moreover, the release of CGA from cGelMA/CGA occurred in a slow and sustained manner (Figure 1G), which could avoid the side effects due to the burst-release stage in the beginning.[47] Notably, the multiple interactions and bonds of CGA further enhance its mechanical properties (Figure 1H). Meanwhile, an ideal CL should provide a comfortable wearer experience, conform to the corneal shape, ensure oxygen permeability, and prevent corneal hypoxic edema.[48] The cGelMA/CGA-CLs has a tunable shape that conformed to the corneal shape, ensuring a comfortable wearer experience (Figure 5). Further, the macroporous structure could circumvent long-term wear causing hypoxic and edematous symptoms, which could ensure comfortable wear as a daily disposable CL material under non-infectious conditions; moreover, in infectious conditions, the cGelMA/CGA-CLs could facilitate complete degradation within 5 h to have timely antibacterial and anti-inflammatory effects (Figures 1D and 1E). So, for daily wearer, cGelMA/CGA could serve as a daily disposable material, and corneal infections can be prevented by controlled and slow CGA release under non-infectious conditions while still ensuring the optical performance needed for the wearing process. For patients who already have a corneal infection, it could be worn overnight for timely materials degradation to fulfill the antibacterial and anti-inflammatory effect. Simultaneously, owing to its highly interconnected pores and high mechanical stability, cGelMA/CGA-CL could also be loaded with

other active ingredients or nonsteroidal anti-inflammatory drugs to achieve better clinical therapeutic effects for other ocular diseases, such as endophthalmitis and graft hyperostosis.

In addition, activated macrophages are the primary contributors to the pathological inflammatory processes and play a critical role in determining the outcomes of BK treatment.[49] Moreover, macrophage depletion in susceptible B6 mice reduces bacterial clearance and increases the severity of BK.[49] Therefore, targeting macrophages to alleviate inflammation and induce bacterial cell death is a practical therapeutic approach. Our study demonstrated that cGelMA/CGA exhibited outstanding antibacterial properties by disrupting bacterial cell membranes, thereby providing a favorable microenvironment for regulating the polarization of macrophages, resulting in significant anti-inflammatory effects (Figure 4E). Importantly, a series of phagocytic receptors are expressed by macrophages that facilitate the internalization of invading pathogens.[50] The RNA-seq data showed that cGelMA/CGA suppressed the expression of inflammatory cytokines and the JAK-STAT signaling pathway in infected macrophages *in vitro* and in infected corneas *in vivo* (Figures 4, 7). The JAK-STAT pathway is essential in the pathogenesis of BK. Moreover, IFN-γ induces LPS responsiveness in HCECs via JAK2-dependent STAT1 activation.[45] Han et al. suggested that targeted inhibition of the JAK-STAT pathway using specific inhibitors might represent a novel therapy for BK.[46] Our study thus was consistent with the reported works. Generally, cGelMA/CGA-CLs exhibited immunoregulatory and antibacterial properties in the treatment of BK, promoting bacterial inflammation clearance by inhibiting the JAK2-STAT1/STAT2 signaling pathway (Figures 3, 4, 6, and 7).

This proof-of-concept study established cGelMA/CGA-CL as a promising alternative to conventional CLs or eye drops in the prevention and treatment integration of ocular infections. However, this study has certain limitations. First, additional assessments using animal models closer to the physiopathology of human eyeballs, such as pigs, are required for further translational development of cGelMA/CGA-CL. Second, cGelMA/CGA-CL should incorporate a silicone component as silicone cryogels to offer the advantage of extremely high oxygen permeability.

EXPERIMENTAL PROCEDURES

Methacrylated gelatin synthesis

Five grams of porcine skin gelatin (type A; Sigma-Aldrich, USA) was dissolved in 50 mL of sustainably stirred Dulbecco's PBS (DPBS; pH = 7.4; Gibco, USA) at 60°C for 5 h. The reaction was conducted for 3 h while 4 mL of methacrylic anhydride (Sigma-Aldrich, USA) was added dropwise to the agitating mixture at a temperature of approximately 50°C. A 5-fold volume of warm water was added to the solution to stop the reaction. After centrifugation at 10,000 rpm for 20 min, the resulting mixture was dialyzed in 12- to 14-kDa molecular-weight cutoff tubing for 1 week against distilled water (dH_2O) with frequent water replacement. The dialyzed solution was lyophilized, and the resulting GelMA polymer was stored at −20°C until use.

Determination of ε-amino groups on GelMA

The amount of ε-amino groups on GelMA was determined using the 2,4,6-trinitrobenzenesulfonic acid (TNBS) assay. One milliliter of GelMA (5 mg/mL) was mixed and reacted with 1 mL of 4% (w/v) $NaHCO_3$ (pH = 8.5) and 1 mL of 0.2% (w/v) TNBS for 4 h at 40°C, following by the addition 3 mL of 6 M HCl. After incubation at 60°C for 2 h, the mixture was diluted using dH_2O, and the absorbance was

measured at 420 nm. The standard curve was established using glycine over a range of concentrations.

GelMA/CGA preparation

The GelMA/CGA conjugate was prepared as follows: 1 mmol of CGA (CGA; MedChemExpress, USA) was dissolved in 10 mL of citrate buffer (pH = 5.5), then 2 mmol of N-hydroxysuccinimide (NHS, Aladdin, China) and 2 mmol of 1-ethyl-3-(30-dimethylaminopropyl) carbodiimide (EDC, Aladdin, China) were successively added to the stirred solution for 20 min at room temperature. The pH of the reaction was raised above 7 using PBS (pH = 7.4). A certain mass of GelMA pre-dissolved in PBS was added to the response. The stirred mixture was allowed to react for 24 h at room temperature. After a sufficient reaction, the solution was dialyzed in dH_2O for 3 days to remove small molecules. The purified conjugate was then freeze-dried and stored in a dryer, avoiding light.

Macroporous GelMA/CGA manufacture

Macroporous GelMA/CGA were dissolved and stirred above lyophilized GelMA thoroughly in DPBS to the final desired concentration of 10% (w/v). A certain amount of potassium persulfate (KPS; Sigma-Aldrich, USA) and tetramethylethylenediamine (TEMED; Sigma-Aldrich, USA) were subsequently added to the solution at concentrations of 0.05% and 0.1%, respectively. This prepolymer solution was pipetted into a six-well plate and placed in a freezer at −20°C. Cryogelation proceeded for 24 h, and the resulting cryogels were thawed before use.

Morphology and elemental analysis

To test for interconnected porosity, formed cryogels were thawed and lyophilized overnight. An SEM (Zeiss, Germany) was used to observe the morphology of the resulting polymer. The dry samples adhered to the conductive tapes and were sprayed with carbon particles. Then, the same magnifications were selected for observation under a voltage of 5 kV. Fourier transform infrared (FTIR) spectroscopic measurements were also performed on a Nicolet-6700 (Thermo Scientific, USA) to study the conjugation of CGA.

Water retention test

A certain weight (W_0) of cryogels was completely dried in the air and measured (W_t). The water content (%) was calculated as follows:

$$\text{Weight content (\%)} = \frac{Wo - Wt}{W0} \times 100\% \qquad \text{(Equation 2)}$$

Degradation behavior

For evaluation of cryogel degradation behavior, wafer-shaped specimens (15 mm in diameter and 1.5 mm in height) were prepared and immersed in 4 mL of 0.1 μg/mL matrix metalloproteinase-2 (MMP-2; Sigma-Aldrich, USA) solutions at 37°C, which was equivalent to the concentration of MMP-2 that was overexpressed in infectious keratitis. The specimen was removed at the specified time, and a Kimwipe was lightly applied to the cryogel surface for 30 s to wick away loosely held water. Subsequently, the weight and morphology were recorded. The weight remaining ratio (%) of the cryogel was calculated as follows:

$$\text{Weight remaining ratio (\%)} = \frac{Wt}{W0} \times 100\% \qquad \text{(Equation 3)}$$

where W_t and W_0 are the weights of the remaining cryogel at time point t and the initial cryogel, respectively.

Swelling behavior

The as-prepared cryogels were immersed in PBS (pH = 7.4) at 37°C to characterize the swelling behavior. The expanded cryogel specimen was removed at set time points and excess moisture was wicked away, weighed, and placed back into the PBS. The process was repeated until a constant weight was achieved. The swelling ratio (%) of the cryogel was calculated as follows:

$$\text{Swelling ratio (\%)} = \left(\frac{Wt}{W0} - 1\right) \times 100\% \quad \text{(Equation 4)}$$

where W_0 is the weight of the initial sample and W_t refers to the weight of the sample after swelling at time point t.

Drug release from cGelMA/CGA

The release of CGA from the cGelMA/CGA cryogel was quantitatively estimated by UV-visible (UV-vis) spectroscopy as follows. A calibration curve was constructed using CGA standards in PBS (pH = 4.8) at concentrations ranging from 0.5 to 250 μg/mL and the absorbance was measured at 324 nm. To determine the release kinetics of CGA, the samples were added to closed dialysis-tubing cellulose membranes containing 80 mL of PBS and dialyzed against the same buffer solution. The different cryogels were incubated in a shaker at 37°C and 250 rpm. At certain time intervals, the amount of CGA released from each cryogel was monitored by removing 2 mL from the buffer solution outside each dialysis membrane. The amount of CGA released at that time was measured using UV-vis spectroscopy as described previously. The sample volume withdrawn from the outer dialysis-bag solution was replaced with a fresh phosphate-buffered solution at each predetermined time interval.

Mechanical properties

For mechanical-property characterization, each specimen was made of cylindrical specimens (11.5 mm in diameter and 8 mm in height). The compression measurements were analyzed using a universal testing machine (Z020; Zwick- Roell, Ulm, Germany) and compressed at 5 mm/min until the cryogels broke. Each sample was repeatedly tested three times.

Cell culture

The HCEC line and human leukemia monocytic cell line (THP-1) were purchased from Meisen Cell Technology (Zhejiang, China). HCECs were cultured in growth medium DMEM/F12 (Gibco, USA) supplemented with 10% (v/v) fetal bovine serum (FBS) (Gibco, USA), 10 ng/mL human epidermal growth factor (hEGF)(Thermo Fisher, USA), 5 μg/mL insulin (Sigma, USA), and 1% antibiotics at 37°C/5% CO_2 and passaged via trypsinization every 2 or 3 days. THP-1 cells were cultured in RPMI 1640 medium (Gibco, USA), supplemented with 10% FBS (Gibco, USA) and 1% penicillin/streptomycin at 37°C in 5% CO_2. THP-1 cells at a density of 1×10^6 cells/well in six- or 24-well plates were differentiated into macrophages after 48 h of treatment with 200 ng/mL phorbol 12-myristate 13-acetate (PMA; Sigma, USA).

Cell proliferation analysis

Cell viability was measured using the CCK-8 assay (Dojindo, WTS, Japan). HCECs were plated in 24-well plates at 5×10^4 cells/well density in 1 mL of complete culture medium and cultured overnight. Transwell chambers containing different cryogels (cGelMA, cGelMA/CGA100, cGelMA/CGA200, and cGelMA/CGA300) were loaded and co-cultured with the cells. The co-cultured solution was carefully transferred into a new 96-well plate after 1, 3, 5, and 7 days of treatment, with 100 μL per well.

Subsequently, 100 μL of the medium was supplemented with 10 μL of CCK-8 solution at 37°C for 2 h under dark conditions. Then, the absorbance value (optical density [OD]) of the mixed solution was read at 450 nm using a microplate spectrophotometer.

Live/dead cell staining

Live/dead staining (Solarbio, China) was performed to assess cell cytotoxicity after direct culture of HCECs with different cryogels for 1 and 7 days. After plating HCECs in 24-well plates at a density of 5×10^4 cells/well, Transwell chambers containing various cryogels were loaded and co-cultured with the cells. At various intervals, the cells were gently rinsed two times with PBS and incubated in the live/dead solution (2 μM calcein-AM and 4.5 μM propidium iodide) for 20 min at 37°C. All experiments were performed in triplicate.

Cell morphological observation

A THUNDER imager scanning microscope (DMI8, Leica, Germany) was used to observe the cell adhesion morphology. Briefly, HCECs were seeded in 24-well plates at a density of 5×10^4 cells/well, cultured for 24 h, gently rinsed three times with PBS, and fixed with 4% paraformaldehyde (PFA) at 25°C for 30 min. Fluorescence staining involved permeabilizing the cells with 0.5% Triton X-100 for 5 min and incubating with rhodamine-phalloidin (Yeason, China) for 30 min at room temperature after washing three times with PBS. Finally, the fixed cells were repeatedly washed with PBS, stained with 4′,6-diamidino-2-phenylindole (DAPI) (Invitrogen, USA) for 5 min, and observed using a THUNDER imager scanning microscopy; three samples were measured for each group.

Bacterial spread plate test

S. aureus and *P. aeruginosa* were used to evaluate the antibacterial activity of the CGA-loaded cryogels. All bacteria were cultivated in Luria-Bertani (LB) medium (Solarbio, China). The bacteria were centrifuged at 5,000 rpm for 5 min, re-suspended in liquid LB medium, and further adjusted to an OD_{600} value of 0.1. Cryogels of each type were added to the Transwell chambers of a 24-well plate and co-cultured with 1 mL of bacterial suspensions (diluting 0.1 OD_{600} to 10^6 CFU/mL). One group treated with the medium alone served as a negative control. *S. aureus* or *P. aeruginosa* (1 mL) (diluted to 10^6 CFU/mL) was cultured without the materials. Subsequently, a direct-inhibition experiment of bacterial growth was conducted after co-incubation for 24 h at 37°C. An aliquot of the co-culture medium was drawn from each well and serially diluted. The viability of *S. aureus* or *P. aeruginosa* was analyzed by evenly coating 100 μL of the serially diluted medium on the agar plates (10^{-3} to 10^{-10}). The number of CFU of *S. aureus* and *P. aeruginosa* was calculated after incubation for a sufficient time. All the groups had three replicates.

Live/dead bacterial fluorescence staining of planktonic bacteria

The total medium was collected after 24 h of incubation and centrifuged at 5,000 rpm for 8 min. Next, the collected bacteria were re-suspended in 100 μL of combination dye (Live/Dead BacLight bacteria viability kits, Invitrogen, USA) and incubated for 15 min. The stained bacterial solution was evenly dispersed on a glass slide and examined under confocal microscopy. Live bacteria with intact cell membranes, dead bacteria, and impaired bacteria with damaged membranes were stained green, red, and yellow, respectively.

Longevity and stability of antibacterial activity

The samples were incubated in liquid LB medium for 12, 24, or 48 h to assess the stability of the antibacterial activity. Different specimens were cultured with the two types of bacterial suspensions at a 10^6 CFU/mL concentration. At each time point, the bacteria were collected and a microplate spectrophotometer measured the OD_{600}. All experiments were performed in triplicate.

Antibiofilm test

In the mature-biofilm destruction test, the bacterial suspension was first inoculated on glass slides of 24-well plates and incubated overnight with LB medium for 24 h to form mature bacterial biofilms. The control group and the experimental group were set up with three compound wells. After culturing for 24 h, the glass slides were slowly rinsed with PBS buffer. Then 500 μL of preprepared Live/Dead dye was added and stained for 15 min at room temperature in the dark. After that, the glass slides were observed for the structure and morphology of bacterial biofilms and the status of living and dead bacteria.

RNA-seq

The RNA sequences of mature THP-1 cells after LPS and cGelMA/CGA_{200} treatment for 24 h were collected using TRIzol reagent (Invitrogen, Carlsbad, CA, USA). Cells without cGelMA/CGA_{200} treatment were used as controls. The concentration of the extracted nucleic acids was checked using a Nanodrop2000 spectrophotometer (Thermo Fisher Scientific), and integrity was checked using an Agient2100, LabChip GX (Platinum, Platinum Elmer LabChip GX). Subsequently, 2 μg of total RNA with a RNA integrity number (RIN) value more significant than seven that met quality control requirements was used for the next step of sequencing library preparation (VAHTS Universal V6 RNA-seq Library Prep Kit for MGI). The library quality was checked using the Qsep-400 method and tested using a HUADA DNBSEQ-T7 gene sequencer. These differentially expressed mRNA functions and possible biological signaling pathways were annotated and hypothesized through GO and KEGG pathway database analyses. RNA-seq data were then entered into the GSEA software (v4.3.2) using the hallmark gene set from the Human Molecular Signatures Database. A false discovery rate (FDR) <0.05, $p < 0.05$ indicated statistically significant enrichment.

Real-time RT-qPCR

Total RNA was extracted from treated THP-1 cells using TRIzol reagent, and the RNA yield was determined by measuring the absorbance at 260/280 nm. A total of 2 μg of RNA was used to generate cDNA with the qPCR RT Master Mix (Toyobo, Osaka, Japan, code no. FSQ-201). Real-time qPCR was conducted using an SYBR Green Real-time PCR Master Mix (Toyobo, Osaka, Japan, code no. QPK-201) with a Real-Time PCR System (Applied Biosystems, Waltham, MA, USA). Relative mRNA expression levels were analyzed using the $2^{-\Delta CT}$ method with GAPDH as an endogenous control and the fold change in expression levels were calculated. All experiments were performed in triplicate. Table S1 lists all the primers.

Protein extraction and WB

Harvested cells were homogenized and lysed in a radioimmunoprecipitation assay buffer containing phosphatase and protease inhibitors. The protein concentration was determined using a bicinchoninic acid (BCA) protein assay kit. Proteins were separated using sodium dodecyl sulfate-polyacrylamide gel electrophoresis and transferred onto polyvinylidene fluoride membranes (Millipore, Billerica, MA, USA) by wet transfer. The membranes were blocked for 20 min with QuickBlock blocking

buffer for WB (Beyotime, Shanghai, China) and incubated overnight at 4°C with the following specific primary antibodies: JAK2 (Abcam, ab108596, 1:1,000 dilution), STAT1 (Proteintech, 10144-2-AP, 1:2,000 dilution), phospho-STAT1 Tyr701 (Proteintech, 28979-1-AP, 1:1,000 dilution), STAT2 (Proteintech, 16674-1-AP, 1:500 dilution), and phospho-STAT2 Y690 (Abcam, ab191601, 1:500 dilution). The membranes were washed three times at 10-min intervals with Tris-buffered saline Tween (TBST) and incubated with diluted secondary antibodies (1:5,000, ZSGB-BIO, Beijing, China) for 1 h at room temperature. The membranes were washed three times with TBST, developed using an enhanced chemiluminescent kit (New Cell & Molecular Biotech, Suzhou, China), and visualized using a multiplex fluorescent imaging system (BLT, GelView 6000Plus, Guangzhou, China).

In vivo BK therapy

C57BL/6J mice (20 mice, half male and half female) were purchased from Beijing Vital River Laboratory Animal Technology. They were housed in an animal room for one week under a 12-h light/dark cycle at a constant temperature with free access to food and water. After 1 week, a BK model construction experiment was initiated. The ocular surface of the mice was observed under a slit lamp to ensure that it was healthy and free from active inflammation before any intervention steps were taken. The mice were fully anesthetized by intraperitoneal injection of freshly configured 1.25% tribromoethanol (0.15 mL/20 g weight). The local anesthetic procaine hydrochloride was administered into the right eye, and the mouse corneal epithelium was scratched using a knife under a stereomicroscope. The scratched area was approximately a circle with a diameter of 2 mm centered on the pupil. After dropping 5 μL of 1×10^8 CFU/mL *S. aureus* solution, infection of the mouse's ocular surface was repeated every 24 h and assessed under a slit lamp after 72 h.

Mice were scored for ocular surface inflammation and corneal clarity to assess the degree of infection. Twenty mice with similar scores were randomly divided into four groups ($n = 5$ per group): (1) control group (PBS, as negative control), (2) clinical LVFX eye drops (5 mg/mL, as positive control), (3) CLs made of cGelMA (cGelMA-CL), and (4) CLs composed of cGelMA/CGA200 (cGelMA/CGA-CL). The CL made of cryogels were degraded within 7 h under infectious conditions. We refitted the mice with a new CL every 24 h. Only this one daily disposable CL-like treatment was given for 24 h, and no further treatments were given in groups 3 and 4. LVFX eye drops were used three times a day, with one drop in each treatment. The progression of keratitis in the mice was subsequently observed under a slit lamp, and the impaired cornea was observed using a corneal fluorescence staining assay (sodium fluorescein staining strips; Jingmingxin, Tian Jin, China; a drop of fluorescein sodium solution was placed into the mouse eye after wetting the fluorescein strip with sterile saline). Photographs were captured every 2 days and recorded on days 1, 3, 5, and 7, respectively.

Clinical scores were assessed on days 1, 3, 5, and 7 according to disease progression to further compare the effect of treatment on keratitis in different groups of mice. The scores were synthetically developed based on the clinical evaluation of postoperative inflammation.[15,18] We used an ocular grading method based on the following four criteria: conjunctival injection and chemosis, hypopyon area, stromal infiltration extent, and corneal and conjunctival epithelial fluorescein staining extent (Table S2). The clinical scores indicated that normal untreated corneas were scored as 0 for each category, resulting in a total score of 0. The scores from all four categories were tallied at 1, 3, 5, and 7 days post -infection for each eye to yield a

possible total score ranging from 0 to 16. The higher the score, the worse the prognosis (Table S2).

This study was approved by the Laboratory Animal Ethics Review Committee of the Faculty of Medicine at Peking University (no. LA2022387), and all animal experiments were conducted following the guidelines of the Committee for the Control and Supervision of Animal Experiments of the Ministry of Public Health of China. All mice were euthanized on day 7, and their eyes were removed for H&E staining and immunohistochemical staining.

Histopathological staining

The cornea was fixed with 4% paraformaldehyde, embedded in paraffin, and sectioned, followed by H&E staining to observe the corneal section. Positive expression of IL-6 (GB11117, Servicebio, China, 1:500 dilution), IL-10 (GB11108, Servicebio, China, 1:100 dilution), JAK2 (A11497, ABclonal, China, 1:100 dilution), p-STAT1 (AP1000, ABclonal, China, 1:100 dilution), STAT1 (10144-2-AP, Proteintech, China, 1:200 dilution), p-STAT2 (bs-3428r, Bioss, China, 1:400 dilution), and STAT2 (16674-1-AP, Proteintech, China, 1:50 dilution) was observed by immunohistochemistry. All the sections were scanned using a panoramic scanner (Pannoramic DESK, P-MIDI, P250; 3D HISTECH, Hungary) at the same magnification (20×) and viewing parameters. Panoramic images of the observed tissue sections were converted into digital images for immunohistochemical analysis. The OD of the immune sections correlated with the expression of positively stained proteins, and the average OD (AOD) was used to analyze the amount of protein expression in each region within the observed sections. The AOD values for different proteins were calculated for all units using ImageJ software (1.53q; NIH, Bethesda, MD, USA).

Statistical analysis

All measurements were made at least in triplicate, and data were presented as mean values ±standard deviation. One-way analysis of variance tests were performed, and differences were considered statistically significant when p values were lower than 0.05: *$p < 0.05$, **$p < 0.01$, ***$p < 0.001$, and ****$p < 0.0001$. The GraphPad Prism 8 statistical software package determined all the statistical analyses.

RESOURCE AVAILABILITY

Lead contact

For additional information or resource requests, please get in touch with the lead contact, Kai Wang, at wang_kai@bjmu.edu.cn.

Materials availability

This study did not generate new unique reagents.

Data and code availability

All data used and analyzed in this study can be found within the article or its supplemental information. No distinctive codes were created for this research. For further details or data required to re-examine the findings of this article, please contact the lead contact.

ACKNOWLEDGMENTS

This work was supported by the National Natural Science Foundation of China (grant nos. 82371087 and 82171092), Capital's Funds for Health Improvement and Research (no. 2022-1G-4083), National Key R&D Program of China (no. 2021YFC2702100). This work was also funded by Young Elite Scientist Sponsorship Program by BAST, the Beijing Training Project for the Leading Talents in S&T (grant no. Z191100006119022), and the National Key Program of the National Natural Science Foundation of China (grant no. 51705006).

AUTHOR CONTRIBUTIONS

Conceptualization, Y.F., F.C., Y.S., Y.L., M.Z., X.Z., and K.W.; investigation, Y.F., F.C., and W.Y.; formal analysis, Y.F., F.C., W.Y., and J.L.; validation, Y.F. and F.C; writing – original draft, Y.F. and F.C; writing – review & editing, X.Z. and K.W., funding acquisition, Y.S., X.Z., and K.W.; supervision, Y.S., Y.L., M.Z., and K.W.

DECLARATION OF INTERESTS

The authors declare no competing interests.

SUPPLEMENTAL INFORMATION

Supplemental information can be found online at https://doi.org/10.1016/j.xcrp.2024.102179.

Received: May 9, 2024
Revised: July 26, 2024
Accepted: August 9, 2024
Published: September 6, 2024

REFERENCES

1. Stapleton, F., Keay, L., Jalbert, I., and Cole, N. (2007). The epidemiology of contact lens related infiltrates. Optom. Vis. Sci. *84*, 257–272. https://doi.org/10.1097/OPX.0b013e3180485d5f.

2. Fleiszig, S.M.J., Kroken, A.R., Nieto, V., Grosser, M.R., Wan, S.J., Metruccio, M.M.E., and Evans, D.J. (2020). Contact lens-related corneal infection: Intrinsic resistance and its compromise. Prog. Retin. Eye Res. *76*, 100804. https://doi.org/10.1016/j.preteyeres.2019.100804.

3. Mutti, D.O., Sinnott, L.T., Berntsen, D.A., Jones-Jordan, L.A., Orr, D.J., and Walline, J.J.; BLINK Study Group (2022). The Effect of Multifocal Soft Contact Lens Wear on Axial and Peripheral Eye Elongation in the BLINK Study. Invest. Ophthalmol. Vis. Sci. *63*, 17. https://doi.org/10.1167/iovs.63.10.17.

4. Zhu, Q., Liu, Y., Tighe, S., Zhu, Y., Su, X., Lu, F., and Hu, M. (2019). Retardation of Myopia Progression by Multifocal Soft Contact Lenses. Int. J. Med. Sci. *16*, 198–202. https://doi.org/10.7150/ijms.30118.

5. Perzia, B., Enzor, R., Kowalski, R.P., and Jhanji, V. (2021). Bilateral Pseudomonas aeruginosa Keratitis in 7 Patients. Eye Contact Lens *47*, 476–479. https://doi.org/10.1097/ICL.0000000000000793.

6. Dart, J.K., Stapleton, F., and Minassian, D. (1991). Contact lenses and other risk factors in microbial keratitis. Lancet *338*, 650–653. https://doi.org/10.1016/0140-6736(91)91231-i.

7. Seal, D.V., Kirkness, C.M., Bennett, H.G., and Peterson, M.; Keratitis Study Group (1999). Population-based cohort study of microbial keratitis in Scotland: incidence and features. Contact Lens Anterior Eye *22*, 49–57. https://doi.org/10.1016/s1367-0484(99)80003-4.

8. Tuft, S., Somerville, T.F., Li, J.-P.O., Neal, T., De, S., Horsburgh, M.J., Fothergill, J.L., Foulkes, D., and Kaye, S. (2022). Bacterial keratitis: identifying the areas of clinical uncertainty. Prog. Retin. Eye Res. *89*, 101031. https://doi.org/10.1016/j.preteyeres.2021.101031.

9. Lin, A., Rhee, M.K., Akpek, E.K., Amescua, G., Farid, M., Garcia-Ferrer, F.J., Varu, D.M., Musch, D.C., Dunn, S.P., and Mah, F.S.; American Academy of Ophthalmology Preferred Practice Pattern Cornea and External Disease Panel (2019). Bacterial Keratitis Preferred Practice Pattern. Ophthalmology *126*, P1–P55. https://doi.org/10.1016/j.ophtha.2018.10.018.

10. Keay, L., Edwards, K., and Stapleton, F. (2009). Signs, symptoms, and comorbidities in contact lens-related microbial keratitis. Optom. Vis. Sci. *86*, 803–809. https://doi.org/10.1097/OPX.0b013e3181ae1b69.

11. Lakhundi, S., Siddiqui, R., and Khan, N.A. (2017). Pathogenesis of microbial keratitis. Microb. Pathog. *104*, 97–109. https://doi.org/10.1016/j.micpath.2016.12.013.

12. Kam, K.W., Yung, W., Li, G.K.H., Chen, L.J., and Young, A.L. (2017). Infectious keratitis and orthokeratology lens use: a systematic review. Infection *45*, 727–735. https://doi.org/10.1007/s15010-017-1023-2.

13. Ung, L., Bispo, P.J.M., Shanbhag, S.S., Gilmore, M.S., and Chodosh, J. (2019). The persistent dilemma of microbial keratitis: Global burden, diagnosis, and antimicrobial resistance. Surv. Ophthalmol. *64*, 255–271. https://doi.org/10.1016/j.survophthal.2018.12.003.

14. Cabrera-Aguas, M., Khoo, P., and Watson, S.L. (2022). Infectious keratitis: A review. Clin. Exp. Ophthalmol. *50*, 543–562. https://doi.org/10.1111/ceo.14113.

15. Hewitt, M.G., Morrison, P.W.J., Boostrom, H.M., Morgan, S.R., Fallon, M., Lewis, P.N., Whitaker, D., Brancale, A., Varricchio, C., Quantock, A.J., et al. (2020). In Vitro Topical Delivery of Chlorhexidine to the Cornea: Enhancement Using Drug-Loaded Contact Lenses and β-Cyclodextrin Complexation, and the Importance of Simulating Tear Irrigation. Mol. Pharm. *17*, 1428–1441. https://doi.org/10.1021/acs.molpharmaceut.0c00140.

16. Huang, J.-F., Zhong, J., Chen, G.-P., Lin, Z.-T., Deng, Y., Liu, Y.-L., Cao, P.-Y., Wang, B., Wei, Y., Wu, T., et al. (2016). A Hydrogel-Based Hybrid Theranostic Contact Lens for Fungal Keratitis. ACS Nano *10*, 6464–6473. https://doi.org/10.1021/acsnano.6b00601.

17. Obuobi, S., Mayandi, V., Nor, N.A.M., Lee, B.J., Lakshminarayanan, R., and Ee, P.L.R. (2020). Nucleic acid peptide nanogels for the treatment of bacterial keratitis. Nanoscale *12*, 17411–17425. https://doi.org/10.1039/d0nr03095c.

18. Zhang, H., Jiang, W., Peng, Y., Yang, J., Chu, X., Long, Z., Li, R., Liang, Q., Suo, H., Wang, S., et al. (2022). Killing three birds with one stone: Near-infrared light triggered nitric oxide release for enhanced photodynamic and anti-inflammatory therapy in refractory keratitis. Biomaterials *286*, 121577. https://doi.org/10.1016/j.biomaterials.2022.121577.

19. Wu, T., and Tang, M. (2018). The inflammatory response to silver and titanium dioxide nanoparticles in the central nervous system. Nanomedicine *13*, 233–249. https://doi.org/10.2217/nnm-2017-0270.

20. Ali, A., Ovais, M., Cui, X., Rui, Y., and Chen, C. (2020). Safety Assessment of Nanomaterials for Antimicrobial Applications. Chem. Res. Toxicol. *33*, 1082–1109. https://doi.org/10.1021/acs.chemrestox.9b00519.

21. Naveed, M., Hejazi, V., Abbas, M., Kamboh, A.A., Khan, G.J., Shumzaid, M., Ahmad, F., Babazadeh, D., FangFang, X., Modarresi-Ghazani, F., et al. (2018). Chlorogenic acid (CGA): A pharmacological review and call for further research. Biomed. Pharmacother. *97*, 67–74. https://doi.org/10.1016/j.biopha.2017.10.064.

22. Lou, Z., Wang, H., Zhu, S., Ma, C., and Wang, Z. (2011). Antibacterial activity and mechanism of action of chlorogenic acid. J. Food Sci. *76*, M398–M403. https://doi.org/10.1111/j.1750-3841.2011.02213.x.

23. Lee, N., Heo, Y.J., Choi, S.-E., Jeon, J.Y., Han, S.J., Kim, D.J., Kang, Y., Lee, K.W., and Kim, H.J. (2021). Anti-inflammatory Effects of Empagliflozin and Gemigliptin on LPS-Stimulated Macrophage via the IKK/NF-B, MKK7/JNK, and JAK2/STAT1 Signalling

Pathways. J. Immunol. Res. *2021*, 9944880. https://doi.org/10.1155/2021/9944880.

24. Clifford, M.N., Jaganath, I.B., Ludwig, I.A., and Crozier, A. (2017). Chlorogenic acids and the acyl-quinic acids: discovery, biosynthesis, bioavailability and bioactivity. Nat. Prod. Rep. *34*, 1391–1421. https://doi.org/10.1039/c7np00030h.

25. Yan, Y., Li, Q., Shen, L., Guo, K., and Zhou, X. (2022). Chlorogenic acid improves glucose tolerance, lipid metabolism, inflammation and microbiota composition in diabetic db/db mice. Front. Endocrinol. *13*, 1042044. https://doi.org/10.3389/fendo.2022.1042044.

26. Lu, H., Tian, Z., Cui, Y., Liu, Z., and Ma, X. (2020). Chlorogenic acid: A comprehensive review of the dietary sources, processing effects, bioavailability, beneficial properties, mechanisms of action, and future directions. Compr. Rev. Food Sci. Food Saf. *19*, 3130–3158. https://doi.org/10.1111/1541-4337.12620.

27. Mazzafera, P., and Robinson, S.P. (2000). Characterization of polyphenol oxidase in coffee. Phytochemistry *55*, 285–296. https://doi.org/10.1016/s0031-9422(00)00332-0.

28. Li, H., Xu, J., Hu, J.-F., Hu, Q.-Y., Fang, X., Sun, Z.-J., Xu, Z., and Zhang, L. (2022). Sustained release of chlorogenic acid-loaded nanomicelles alleviates bone loss in mouse periodontitis. Biomater. Sci. *10*, 5583–5595. https://doi.org/10.1039/d2bm01099b.

29. Eggermont, L.J., Rogers, Z.J., Colombani, T., Memic, A., and Bencherif, S.A. (2020). Injectable Cryogels for Biomedical Applications. Trends Biotechnol. *38*, 418–431. https://doi.org/10.1016/j.tibtech.2019.09.008.

30. Memic, A., Colombani, T., Eggermont, L.J., Rezaeeyazdi, M., Steingold, J., Rogers, Z.J., Navare, K.J., Mohammed, H.S., and Bencherif, S.A. (2019). Latest Advances in Cryogel Technology for Biomedical Applications. Advanced Therapeutics *2*, 1800114. https://doi.org/10.1002/adtp.201800114.

31. Bencherif, S.A., Sands, R.W., Bhatta, D., Arany, P., Verbeke, C.S., Edwards, D.A., and Mooney, D.J. (2012). Injectable preformed scaffolds with shape-memory properties. Proc. Natl. Acad. Sci. USA *109*, 19590–19595. https://doi.org/10.1073/pnas.1211516109.

32. Newland, B., Welzel, P.B., Newland, H., Renneberg, C., Kolar, P., Tsurkan, M., Rosser, A., Freudenberg, U., and Werner, C. (2015). Tackling Cell Transplantation Anoikis: An Injectable, Shape Memory Cryogel Microcarrier Platform Material for Stem Cell and Neuronal Cell Growth. Small *11*, 5047–5053. https://doi.org/10.1002/smll.201500898.

33. Tavakol, D.N., Tratwal, J., Bonini, F., Genta, M., Campos, V., Burch, P., Hoehnel, S., Béduer, A., Alessandrini, M., Naveiras, O., and Braschler, T. (2020). Injectable, scalable 3D tissue-engineered model of marrow hematopoiesis. Biomaterials *232*, 119665. https://doi.org/10.1016/j.biomaterials.2019.119665.

34. Filippova, A., Bonini, F., Efremova, L., Locatelli, M., Preynat-Seauve, O., Béduer, A., Krause, K.-H., and Braschler, T. (2021). Neurothreads: Development of supportive carriers for mature dopaminergic neuron differentiation and implantation. Biomaterials *270*, 120707. https://doi.org/10.1016/j.biomaterials.2021.120707.

35. Li, J., and Mooney, D.J. (2016). Designing hydrogels for controlled drug delivery. Nat. Rev. Mater. *1*, 16071. https://doi.org/10.1038/natrevmats.2016.71.

36. Yazdanpanah, G., Shen, X., Nguyen, T., Anwar, K.N., Jeon, O., Jiang, Y., Pachenari, M., Pan, Y., Shokuhfar, T., Rosenblatt, M.I., et al. (2022). A Light-Curable and Tunable Extracellular Matrix Hydrogel for In Situ Suture-Free Corneal Repair. Adv. Funct. Mater. *32*, 2113383. https://doi.org/10.1002/adfm.202113383.

37. Wei, S., Yin, R., Tang, T., Wu, Y., Liu, Y., Wang, P., Wang, K., Mei, M., Zou, R., and Duan, X. (2019). Gas-Permeable, Irritation-Free, Transparent Hydrogel Contact Lens Devices with Metal-Coated Nanofiber Mesh for Eye Interfacing. ACS Nano *13*, 7920–7929. https://doi.org/10.1021/acsnano.9b02305.

38. García-López, C., Rodríguez-Calvo-de-Mora, M., Borroni, D., Sánchez-González, J.-M., Romano, V., and Rocha-de-Lossada, C. (2023). The role of matrix metalloproteinases in infectious corneal ulcers. Surv. Ophthalmol. *68*, 929–939. https://doi.org/10.1016/j.survophthal.2023.06.007.

39. Papas, E.B., Chiem, A., Zhang, G., Mobeen, R., and Lee, L. (2021). Temporal considerations in contact lens discomfort. Contact Lens Anterior Eye *44*, 14–17. https://doi.org/10.1016/j.clae.2020.08.007.

40. Chaudhari, P., Ghate, V.M., and Lewis, S.A. (2021). Next-generation contact lenses: Towards bioresponsive drug delivery and smart technologies in ocular therapeutics. Eur. J. Pharm. Biopharm. *161*, 80–99. https://doi.org/10.1016/j.ejpb.2021.02.007.

41. Hosseinian, H., Hosseini, S., Martinez-Chapa, S.O., and Sher, M. (2022). A Meta-Analysis of Wearable Contact Lenses for Medical Applications: Role of Electrospun Fiber for Drug Delivery. Polymers *14*, 185. https://doi.org/10.3390/polym14010185.

42. Ljubimov, A.V., and Saghizadeh, M. (2015). Progress in corneal wound healing. Prog. Retin. Eye Res. *49*, 17–45. https://doi.org/10.1016/j.preteyeres.2015.07.002.

43. Jiang, Y., Kusama, K., Satoh, K., Takayama, E., Watanabe, S., and Sakagami, H. (2000). Induction of cytotoxicity by chlorogenic acid in human oral tumor cell lines. Phytomedicine *7*, 483–491. https://doi.org/10.1016/s0944-7113(00)80034-3.

44. Ivashkiv, L.B. (2018). IFNγ: signalling, epigenetics and roles in immunity, metabolism, disease and cancer immunotherapy. Nat. Rev. Immunol. *18*, 545–558. https://doi.org/10.1038/s41577-018-0029-z.

45. Roy, S., Sun, Y., and Pearlman, E. (2011). Interferon-gamma-induced MD-2 protein expression and lipopolysaccharide (LPS) responsiveness in corneal epithelial cells is mediated by Janus tyrosine kinase-2 activation and direct binding of STAT1 protein to the MD-2 promoter. J. Biol. Chem. *286*, 23753–23762. https://doi.org/10.1074/jbc.M111.219345.

46. Han, F., Guo, H., Wang, L., Zhang, Y., Sun, L., Dai, C., and Wu, X. (2020). TSLP Produced by Aspergillus fumigatus-Stimulated DCs Promotes a Th17 Response Through the JAK/STAT Signaling Pathway in Fungal Keratitis. Invest. Ophthalmol. Vis. Sci. *61*, 24. https://doi.org/10.1167/iovs.61.14.24.

47. Behne, S., Franke, H., Schwarz, S., and Lachenmeier, D.W. (2023). Risk Assessment of Chlorogenic and Isochlorogenic Acids in Coffee By-Products. Molecules *28*, 5540. https://doi.org/10.3390/molecules28145540.

48. Papas, E.B. (2014). The significance of oxygen during contact lens wear. Contact Lens Anterior Eye *37*, 394–404. https://doi.org/10.1016/j.clae.2014.07.012.

49. Hazlett, L.D. (2004). Corneal response to Pseudomonas aeruginosa infection. Prog. Retin. Eye Res. *23*, 1–30. https://doi.org/10.1016/j.preteyeres.2003.10.002.

50. Yang, K., Wu, M., Li, M., Li, D., Peng, A., Nie, X., Sun, M., Wang, J., Wu, Y., Deng, Q., et al. (2014). miR-155 suppresses bacterial clearance in Pseudomonas aeruginosa-induced keratitis by targeting Rheb. J. Infect. Dis. *210*, 89–98. https://doi.org/10.1093/infdis/jiu002.